Past, Present and Climate Change Scenarios: Investigating Erosion Risk on Archaeological Heritage in the Sinni Valley (Basilicata, Italy)

Antonio Minervino Amodio, Maria Danese(✉), and Dario Gioia

ISPC-CNR, Tito Scalo 87050, Potenza, Italy
maria.danese@cnr.it

Abstract. Erosion is one of the main hazard factors for archaeological heritage; consequently, it is important to monitor it in the past and in its current distribution and to forecast its evolution in the future. Climate changes and its effects alter this last, in particular depending on rains. Consequently, in this paper, the USPED model is used to calculate erosion for different years; moreover, a simulation of future development is proposed. This in order to investigate the erosion risk on the archaeological heritage in the Sinni Valley, a place rich of sites and traces of the past.

Keywords: Erosion · climate changes · archaeological heritage · spatial analysis

1 Introduction

In the context of conservation of cultural heritage, a critical factor is the complex interaction between archaeological sites and environment. Consequently, implication for the territory deriving from climate changes and the increased vulnerability of archaeological heritage became a topic of primary importance [1–6].

Generally, a fragile territory, subject to natural hazard, is a threat also for cultural heritage [7, 8] because it favors:

- the destruction of the cultural identity represented by individual landscapes;
- the removal of archaeological traces and findings in areas not yet investigated;
- the damages to cultural heritage exposed to sources of risk.

In particular climate changes contribute to increase hazard by causing the following impacts [7]: sea level rise, flooding, erosion along the coast, temperature changes in the air and sea, variations in humidity, harsh weather, weathering, and modifications to the conditions of the soil and sediment.

Between all these, in this paper we focus on erosion and how climate changes can affect it and, consequently, cultural heritage.

Erosion is an element of danger for both the visible and the unexcavated archaeological heritage [9–12], so it is important to effectively model and map it, by simulating variable scenarios as weather conditions vary from a regular situation.

© The Author(s), under exclusive license to Springer Nature Switzerland AG 2024
O. Gervasi et al. (Eds.): ICCSA 2024 Workshops, LNCS 14819, pp. 412–428, 2024.
https://doi.org/10.1007/978-3-031-65282-0_27

Future climate change is expected to present significant difficulties for heritage management, particularly in landscape contexts such as river valleys. The magnitude, intensity, and character of geomorphological processes are likely to change in response to shifting threshold conditions. Landscapes with archaeological sites pose specific challenges to heritage professionals, not only because of the close association of historical remains with the physical environment, but also because in these landscapes erosion and soil denudation phenomena often affect the cultural heritage.

In recent years, advances in IT have led to the proliferation of physics-based predictive models aimed at quantitative investigation of soil erosion and sediment flux assessments in basins [13], which, however, have shown controversial results and poor reliability, due in part to the difficulty of parameter estimation and their local validity. Therefore, their application is limited to small areas where a large amount of data is available. Instead, the USPED (Unit Stream Power-based Erosion Deposition) model is semi-physical based on a more simplified and conceptual approach that focuses on water stream energy as the main driver of soil erosion that has returned good results in the literature [14].

The aim of this paper is, consequently, to study the evolution of erosion in the Sinni Valley in the last thirty years and to foresee how it will evolve in the future by considering the effects of climate changes according to the scenarios envisaged by IPCC (Intergovernmental Panel on Climate Change). This in order to highlight areas most subjected to erosion and archaeological heritage susceptible by it at the present and in the future and to contribute also to the management of archaeological heritage in the practice, for a planning and a programming aimed to their conservation or however for risk mitigation.

The paper is structured as follows: in Section 2 the methods used are introduced, in Section 3 the case study of the Sinni Valley and its archaeological heritage are presented; finally in Section 4 the vulnerability assessment and the application of USPED are showed, before the final discussion in Section 5.

2 Methods

2.1 Spatial Analysis: Nearest Neighbor Methods and Kernel Density Estimation

To determine vulnerability areas, in this paper two methods were used. For the practical description, see Sect. 4.

Nearest Neighbor (NN) methods are the most common distance-based methods (distance d between each couple of s_i and s_j elements) and provide information on the interaction between the n events at the local level.

By calculating the NN Observed Distance (NNOD, Eq. 1), the NN Expected Distance (NNES, Eq. 2), the NN Index (NNI, Eq. 3) and by comparing this last with the z-score and p-value of the distribution, it is possible to understand if events are distributed in a random or clustered way over the space. NNI shows positive spatial autocorrelation if it tends to 1, if the p-value (probability that a spatial process is created randomly) is very small and the z-score (number of standard deviations) is very high or very small. This, in the case of vulnerability, is useful to understand, in presence of clusters, if the area

between sites have a greater probability to be vulnerable from the archaeological point of view.

$$\text{NNOD} = \frac{\sum_{i=1}^{n} d_{min}}{n} \tag{1}$$

$$NNED = 0.5\sqrt{\frac{A}{n}} \tag{2}$$

$$\text{NNI} = \frac{\text{NNOD}}{\text{NNED}} \tag{3}$$

Kernel Density Estimation (KDE) uses a three-dimensional moving function to weight events by their distance from the point at which the intensity is estimated. KDE is commonly used in statistical contexts to obtain smooth estimates of univariate or multivariate probability densities. KDE (Eq. 4) is always nonnegative and depends on key parameters such as grid resolution, kernel function (k), the intensity (L) and especially bandwidth (τ). For a complete description of KDE see [15].

$$\lambda(L) = \sum_{i=1}^{n} \frac{1}{\tau^2} k\left(\frac{L - L_i}{\tau}\right) \tag{4}$$

2.2 USPED Method for Erosion Estimation

The USPED model was applied to simulate erosion scenarios in different years: in 1990, in 2000, in 2015, in 2023, in 2023 but considering a climate change scenario (ccs) with land use of 2023 and simulations of extreme events in the rainfall series as explained further.

USPED model uses the structure of the empirical Revised Universal Soil Loss Equation (RUSLE) to calculate the average soil loss (A). The 2-dimensional USPED model of erosion was created with an assumption that erosion and deposition are principally dependent from the sediment transport capacity of surface runoff.

In particular, the following equation (Eq. 5) was used [16]:

$$A = R \cdot K \cdot LS \cdot C \cdot P \tag{5}$$

where: A is the annual average soil loss, R is the rainfall intensity factor, K is the soil erodibility factor, L is the slope length factor, S is the slope steepness factor, C is the land cover factor, P is the soil conservation or prevention practice factors.

The formula is based on the upslope contributing area. It considers the tangential (perpendicular to the downhill direction) curvature as well as the profile (downhill direction) [17].

Net erosion or deposition (ED) within a grid cell is computed as the divergence of sediment flow (change in sediment transport capacity) using Eq. 6, where α is the terrain's aspect (in degrees).

$$ED = \partial[(A \cdot cos\alpha)/\partial x] + \partial[(A \cdot sin\alpha)/\partial y] \tag{6}$$

According to the physical basis of the model, net erosion pixels correlate with profile convexity and tangential concavity (flow acceleration and convergence), while net deposition pixels correlate with profile concavity (decreasing flow velocity).

The parameters of rainfall and runoff, which are influenced by height and location, define the R factor. This was determined by applying an empirical Eq. (7) [18] tested in [14, 19] where *EI30* is the rainfall erosivity (MJ mm h − 1 ha − 1 yr − 1) and P_{24} is the daily rainfall amount (mm).

$$EI30 = 0.1087(P_{24})^{1.36} \tag{7}$$

Equation 7 was calculated using daily precipitation data for the period from 2000 to 2020.

To simulate the effects of climate change on the rainfall series, some daily values were modified. In particular, for each month, a higher (one-day) rainfall event was introduced by summing the rainfall of a 3–4 or 5-day rainfall event. In this way, by condensing the rainfall amount of several days into one day, the final rainfall amount does not change, but the value of the R-factor changes, which follows the behavior of Eq. 7. In this way today's rainfall events are simulated, in which greater amounts of rain fall in a more closely spaced manner.

Using a standard Wischmeier erosion plot [20], the soil erodibility factor (K) was calculated as the rate of soil loss per rainfall erosion index unit (Mg h MJ^{-1} mm^{-1}).

Equation 8 determines the K factor, which shows how the soil profile responds to erosive force of rainfall events:

$$K = 0.001317\Big[2.1 \cdot 10^{-4}(12 - M)\Big[(Si + f_S)(100 - c)]1.14 + 3.25(a - 2) + 2.5(P - 3)] \tag{8}$$

In Eq. 8 M is the organic matter content (%), Si is the silt fraction in % (2 to 50 μm), f_S is the fine sand content in % (50 to 100 μm), c is the clay content in % (less than 2 μm), a is the structure, P is the permeability class (within the top 0.60–0.70 m); factor 0.001317 is derived via division by 100 of the conversion value (0.1317) to the SI.

Data on texture, structure, and permeability were taken from previous researches [21, 22] that examined the physical and chemical characteristics of deposit outcropping in the southern Apennine chain's foredeep area.

The topographic factor LS (dimensionless) was determined using Eq. 9, where Ac is the upslope contributing area per unit of width (m), α_0 is the length (72.6 ft, equal to 22.13 m) of the standard terrain, β_0 is the angle (9%, equal to a 5.16 slope degree) of the standard terrain, m and n (0.6 and 1) are empirical exponents [16].

$$LS = (m + 1) \cdot (A_c/\alpha_0)^m \cdot sin(\beta_0/0.0896)^n \tag{9}$$

The topographic parameters were calculated using a 5 m DEM collected from geoportals of the Basilicata and Calabria Regions.

The C factor, which indicates how crops and management practices affect soil erosion rates, was computed using values assigned based on vegetation cover, density and type of cover, according to literature data [23, 24]. Different C-factors were used for modelling scenarios in different annualities, in particular, land uses of 1990, 2000, 2015 and 2023

were used. The years 1990 and 2000 are derived from Corine Land Cover (CLC), while 2015 and 2023 are derived from Dynamic World (DW) data (satellite land-use data with a pixel resolution of 10 m. The P-factor does not vary in the study area; therefore, its value is assumed to be equal to one.

3 Study Area

3.1 The Sinni Valley

The Sinni Valley is a region located in the southern part of Basilicata, Italy (Fig. 1). The entire valley is crossed by the Sinni River, which finds in it the extension of almost its entire basin. The Sinni River largely traverses the Southern Apennines from west to east. In the lower section, after deeply incising a NNW-SSE-trending morphostructure of the Apennines (known as the Valsinni Ridge), the river flows with a wide deviation toward the southeast, passing through the internal sector of the Bradanic foredeep before emptying into the Ionian Sea near Policoro. In the intermediate section, the Sinni River and its major tributaries—the Sarmento River and the Serrapotamo Stream—cross the southern part of the Pliocene-Pleiscocene Sant'Arcangelo Basin [25]. This basin represents a tectonic depression bounded to the southwest by the Pollino Massif, Monte Alpi, and Monte Raparo, and to the northeast by the Valsinni Ridge, which separates the basin from the Bradanic Foredeep. The area occupied by the Sinni basin is 1343 km^2 and varies in elevation from 0 to 2247 m.

3.2 The Archaeological Map of the Sinni Valley and Vulnerability Criteria

The Sinni Valley is a region rich in history and archaeological sites that testify human occupation since ancient times. These sites include prehistoric settlements, necropolises, Roman settlements, medieval churches, castles, and many other archaeological features. Indigenous people have inhabited the area since prehistoric times, as evidenced by outcrops of lithic artifacts and the remains of dwellings. This study region is interesting because of the variety of archaeological sites in terms of both typology and chronological, being wide and favorable for population, both because of its landscape and the proximity to two large cities, Siris and Heraclea.

For this article, data from the Archaeological Map of the Middle and Upper Sinni Valley, entrusted in the years 1996–2003 to the Chair of Ancient Topography at the Second University of Naples and the Chair of Topography of Ancient Italy at the University of Bologna, were used [26–33]. Overall in the studied area we mapped 1014 sites.

For what concerns the vulnerability of the study area, different classes were identified according to criteria discussed by [34] (Fig. 1):

- Minimum protection priority classes: classes in which what found is unlikely to imply the possibility of having additional buried items. These are terracing, sporadic frequentation, spring, agricultural shelter, lookout, for a total of 14 sites.
- Classes with medium protection priority: classes in which it is not certain, but it may well be the case, that further investigation will lead to the presence of additional features beyond those known, thus not yet excavated or investigated by geophysics. These are materials, necropolis, kiln, tomb, for a total of 664 sites.

– Classes with high protection priority: classes in which elements of archaeological interest are actually already present or in which it is possible, through further investigation, to discover additional elements of interest. They are farm, habitation, settlement, castle, fortification, shrine, structure, monastery, rustic house, abbey, cave, mule track, villa, aggregate, church, castling, fortified town, monastic settlement, street, rustic settlement, cult building, for a total of 337 sites.

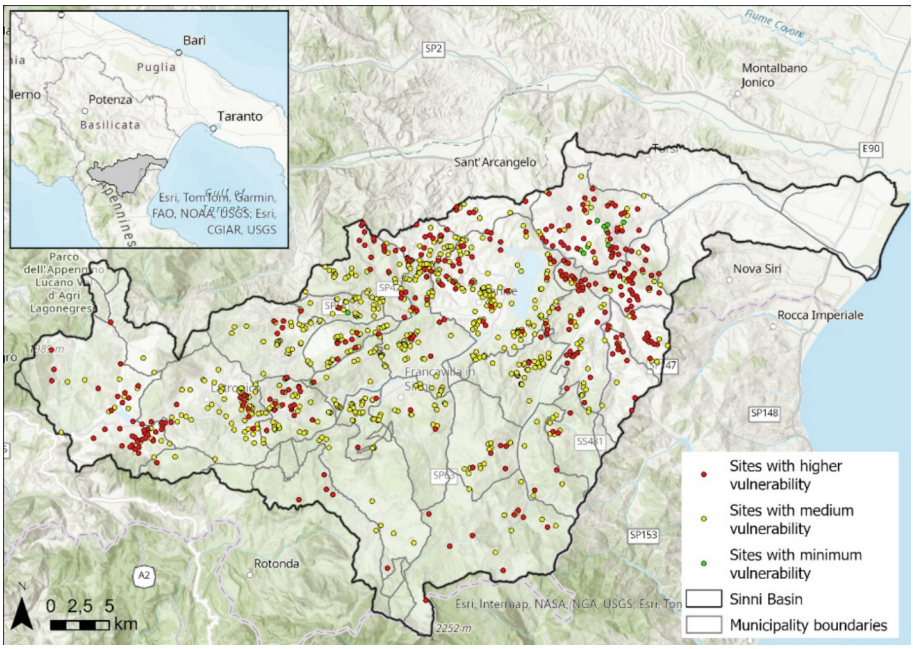

Fig. 1. The study area: the Sinni Valley sites and the catchment of the Sinni River.

4 Results

4.1 Vulnerability Assessment

With the purpose of estimating erosion in the past, at the present and under a future scenario modified by climate change, the first step consisted in computing at risk areas.

Consequently, the three classes of sites characterized by a different vulnerability level of vulnerability, as defined in the previous paragraph, were investigated with the NNIs and KDE, in order to obtain vulnerability areas. According to the NNI found, the z-score and the p-value (Table 1), it emerges that sites with minimum vulnerability have a random distribution, while sites with medium and maximum vulnerability have a clustered distribution.

Afterwards, the NNED were introduced as bandwidth for KDE, in order to find areas more vulnerable, from the archaeological point of view, by erosion (Fig. 2). For

what concerns the other KDE parameters: the sum of the occurrences of each site in the different epochs was used as the intensity; a cell size of five meters was set; the Epanechnikov's kernel was chosen, in order to consider a finite spatial relationship between the sites. The KDE results (Figs. 2, 3, 4) were classified in quantiles. For the sites with minimum vulnerability two classes were sufficient, instead for the medium and maximum vulnerability five classes were highlighted.

Table 1. NNIs found for the three classes of sites with different vulnerability level.

Index	Sites with minimum vulnerability	Sites with medium vulnerability	Sites with maximum vulnerability
NNOD (m)	1685,74	400,71	681,63
NNED (m)	2017,03	753,79	1106,61
NNI	0,84	0,53	0,62
z-score	-1,13	-23,09	-13,49
p-value	0,26	0	0

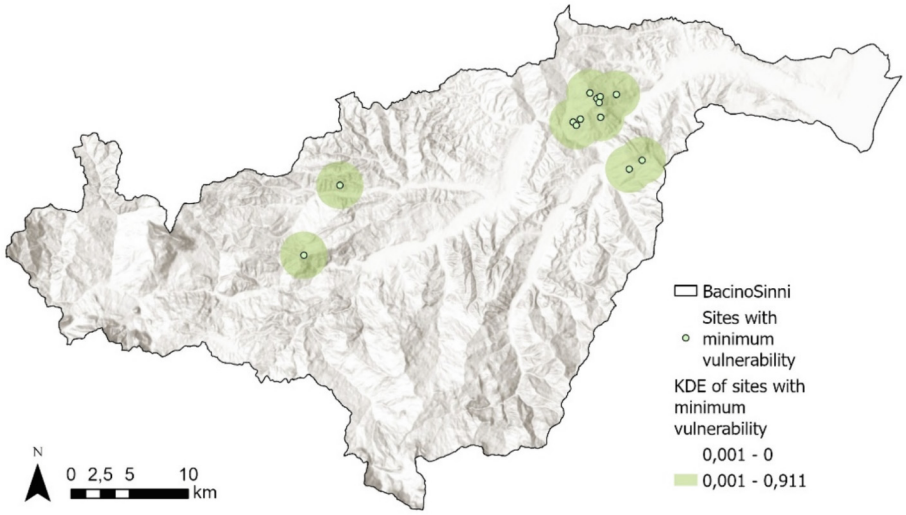

Fig. 2. KDE for sites with minimum vulnerability.

Here a limitation of this method appears, because a better way to proceed to find vulnerability areas would be to use, instead of a simple area of influence, predictive archaeological models [35, 36] calibrated for each historical era identified within the sites and taking into account the different environmental parameters present in the study area. However, the KDE is sufficient for a rough estimation of how much erosion affects the distribution of clustered sites such as these and their landscape context.

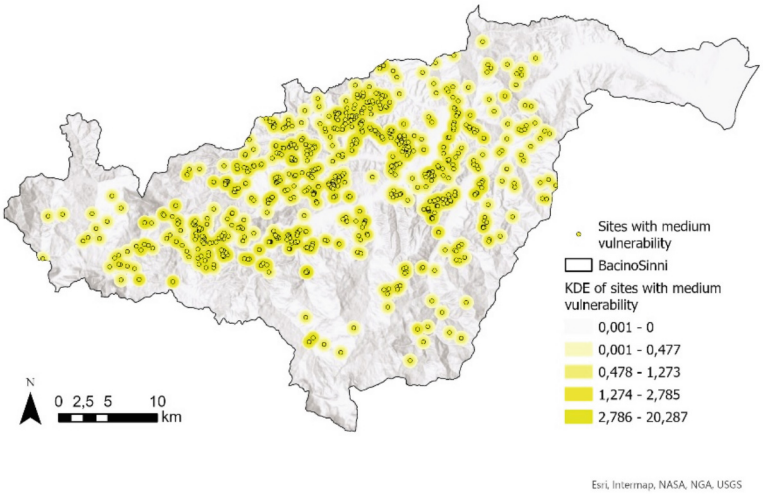

Fig. 3. KDE for sites with medium vulnerability.

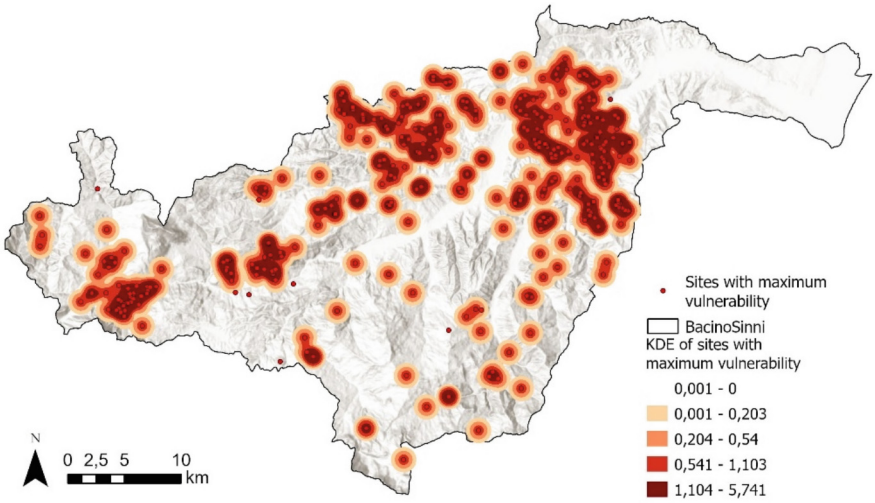

Fig. 4. KDE for sites with maximum vulnerability.

4.2 USPED Computation

For USPED computation, the following parameters were calculated:

1 The study area was classified, for each period, into eight land-use classes: (1) urban, industrial, and commercial area; (2) arable land; (3) fruit tree, vineyard, and olive groves; (4) pastures and natural grasslands; (5) forest area; (6) water. Values were assigned to these classes for the calculation of the c-factor for the different years with values used in the literature [14].

2 The rainfall intensity factor (*R* factor) was calculated taking into account a time range from 2000 to 2020 for 21 stations: Agromonte, Armento, Carbone, Castelluccio Inferiore, Castelsaraceno, Cersosimo, Cogliandrino, Lagonegro, Lauria, Missanello, Noepoli, Nova Siri, Nova Siri Scalo, San Giorgio Lucano, San Severino Lucano, Senise, Terranova del Pollino, Trecchina, Tursi, Valsinni and Viggianello.
3 The soil erodibility factor (K factor) was derived from lithological information [37] and shows a range between 0.15 and 0.35.

The slope length and steepness factor map (LS factor) shows a value between 0 and 1700.

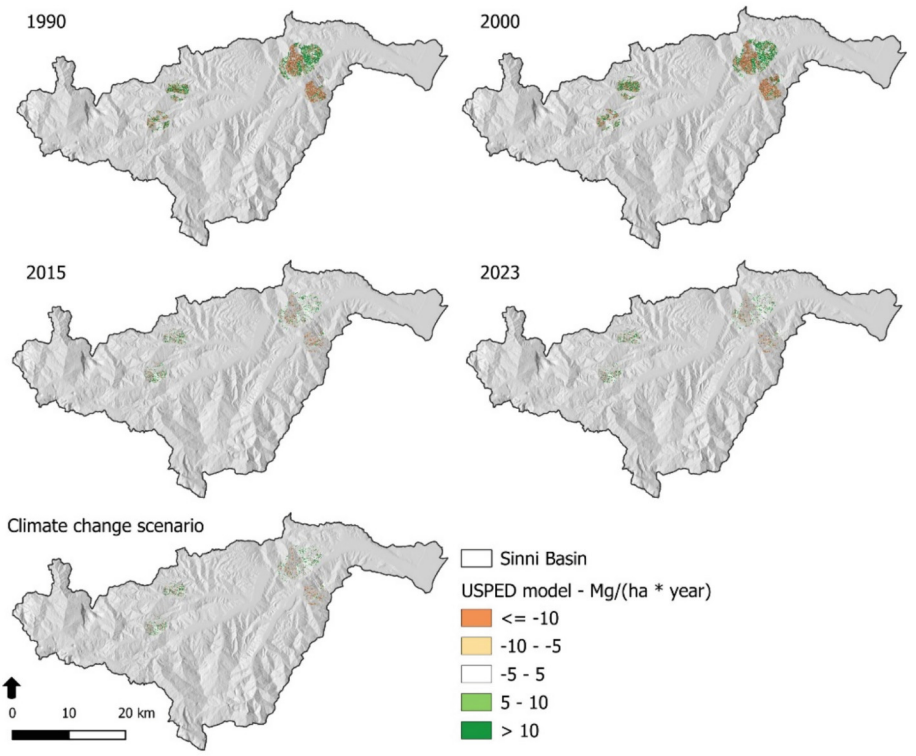

Fig. 5. USPED model for different year and scenarios inside areas with minimum level of vulnerability.

After the erosion simulation using the USPED model, the scenarios were derived from the different input data in the years 1990, 2000, 2015, 2023 and in case of climate changes (Ccs). The difference between the various scenarios depends on the land use at the reference year (c-factor), except for USPED Ccs, which compared to USPED 2023 changes the value of the R-factor taking into account more concentrated and intense rainfall than the current situation.

For all USPED map each pixel was categorized using the five erosion/deposition classes listed below:

- High erosion (<-10 Mg ha^{-1} yr^{-1});
- Low erosion ($-10/-5$ Mg ha^{-1} yr^{-1});
- Stable ($-5/5$ Mg ha^{-1} yr^{-1});
- Low deposition (5/10 Mg ha^{-1} yr^{-1});
- High deposition (>10 Mg ha^{-1} yr^{-1}).

The USPED maps from five distinct periods were overlaid onto maps depicting the vulnerability levels of archaeological sites. The three erosion scenarios for the three vulnerability classes were obtained in this way, resulting the maps in Figs. 5, 6 and 7.

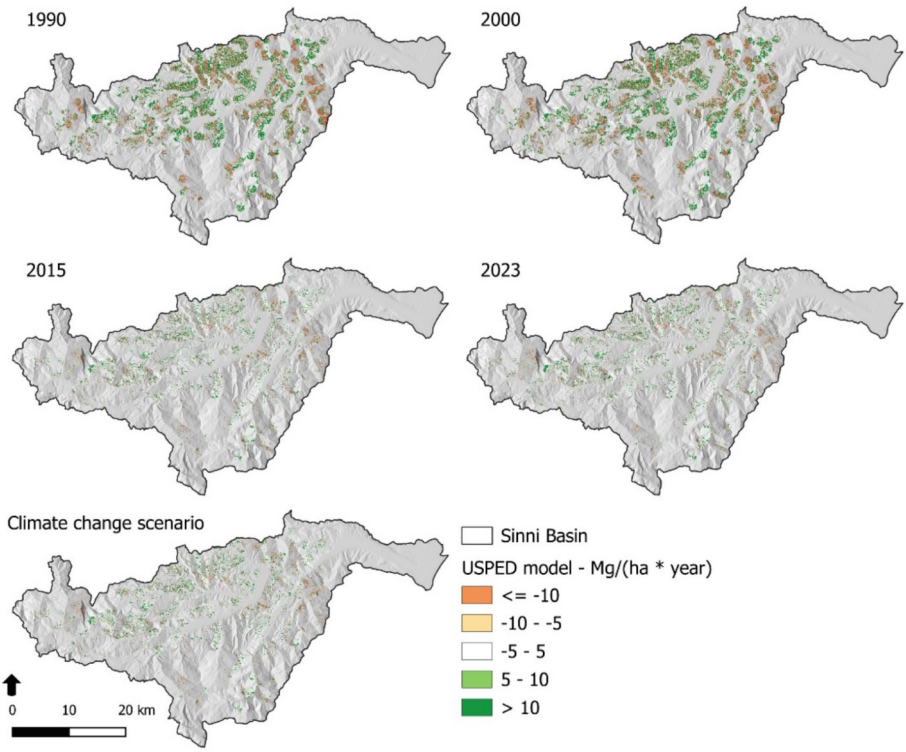

Fig. 6. USPED model for different year and scenarios inside areas with medium level of vulnerability.

The results obtained, depicted in Table 2, show two different behaviors. 1990 and 2000 show values for the stable class for sites with maximum vulnerability of about 28500 hectares, which are significantly lower than the values in 2015, 2023 and Ccs of about 41000 hectares. This trend is also similar for the other two vulnerability classes. The period 1990/2000, having a smaller amount of stable soil, have a larger amount of soil in erosion and deposition than the years 2015, 2023 and Ccs.

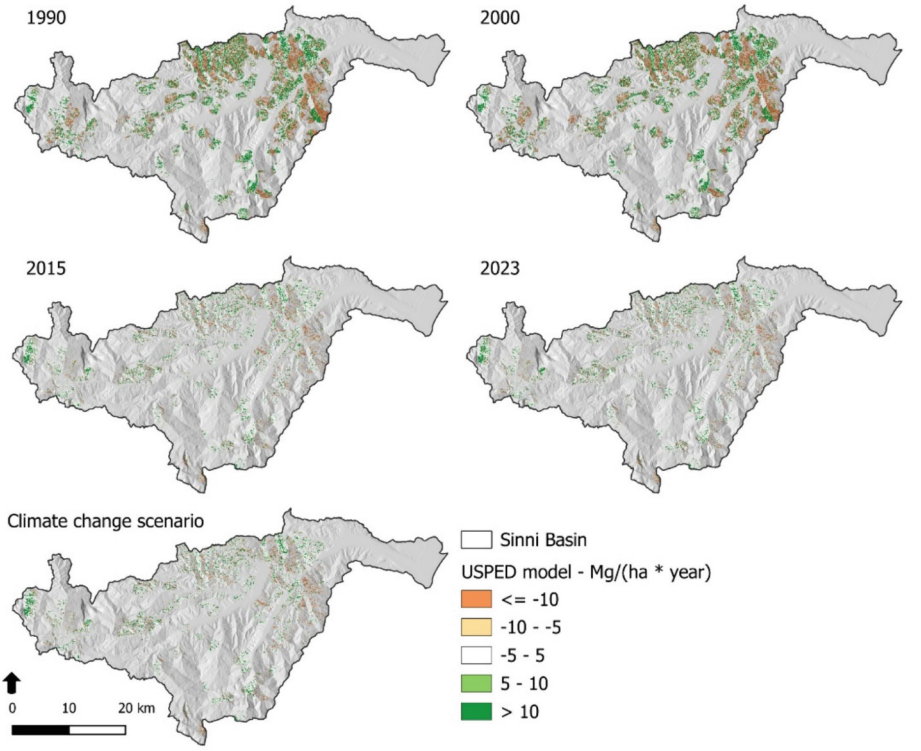

Fig. 7. USPED model for different year and scenarios inside areas with maximum level of vulnerability.

In fact, always taking into account the "maximum vulnerability" class in erosion, we go from about 8500 ha for 1990 and 1700 to about 2000 ha for 2015, 2023 and Ccs. While for deposition in the same vulnerability class it goes from about 9000 ha in 1990 and 2800 to about 3200 ha in the other years taken into account. The trend for the other vulnerability classes is similar.

This different behavior of the two sets of years is due to two different reasons, the first one to the nature of the input data in the USPED model and the second one to the change in land uses. The first difference derives from the different nature of the input data in the c-factor calculation. In fact, for 1990 and 2000, as land-use the CLC dataset was employed; this has a smaller scale and therefore a greater degree of uncertainty and a larger base pixel with a lower capacity to represent the single object (e.g. land-use change). While for the years 2015 and 2023 (also for Ccs, having the same land-use as 2023) the input data have a better resolution and consequently also a better representation of reality. The second reason that causes this difference in the dataset (pragmatically to a smaller extent than the previous one) is the change in land use over time. As time goes by, there is an increasing tendency for inland areas, which were previously used for agriculture, to be abandoned, with uncontrolled growth of vegetation. This results in a soil protection effect that tends to decrease erosion and soil deposition.

Table 2. Resulting USPED inside vulnerability areas in hectares for the different scenarios.

	1990			2000			2015			2023			Ccs		
Classes	Min vuln	Med vuln	Max vuln	Min . Vuln	Med vuln	Max vuln	Min vuln	Med vuln	Max vuln	Min vuln	Med vuln	Max vuln	Min vuln	Med vuln	Max Vuln
High erosion	1693	7694	8471	1850	7907	8570	433	1791	2027	358	1769	1988	405	1996	2238
Low erosion	209	1047	1104	197	1091	1159	173	810	883	164	807	894	173	843	938
Stable	4444	27693	28545	4247	27430	28463	6804	40090	41744	6970	40096	41802	6860	39509	41160
Low depos	199	1136	1229	196	1195	1270	188	1102	1151	171	1053	1115	175	1066	1138
High depos	1536	8830	9336	1591	8778	9225	484	2610	2857	419	2678	2888	469	2988	3213

5 Discussion and Final Remarks

A practical and affordable way to safeguard historically and culturally significant archaeological sites and monuments from environmental and human interference consists of preventive preservation and monitoring. Climate change may amplify cultural heritage exposure to climatic stressors by causing gradual changes in climate, sea level rise, and the occurrence of extreme weather events. In studies issued more than a decade ago, UNESCO underlined the need for greater research on such impacts [38, 39], and as a result, the number of published articles on this topic increased. Cultural heritage can be severely impacted by landslides, flooding, rising sea levels and the effects they have on coastal communities, and other catastrophic changes in the physical environment brought on by climate change [8]. One of the most significant effects of climate change on Europe's cultural heritage is flooding [40]. Europe is expected to see more frequent and larger floods, [41]identified areas that are especially vulnerable. Floods damage various heritage typologies in coastal locations by compounding other losses [42–45].

Increasing storm surge frequency and sea level rise will exacerbate coastal erosion, reshaping the shoreline, and increase the frequency of coastal flooding, which will affect coastal heritage sites. Climate change may increase the effects of eolian and marine processes, such as wave action and currents, on shoreline and submerged archeological sites, increasing erosion and perhaps leading to the collapse of cultural constructions [46]. The reshaping of the beach can affect several heritage typologies, some of which may disappear owing to erosion [47] and coastal retreat, but also due to silt accumulation.

Water-induced soil erosion is one of the main environmental hazards that has put several ancient sites in the Mediterranean region in danger. The detaching, transporting, and depositing of soil sediment on a site can be directly impacted by soil erosion; therefore learning about these two processes is crucial to the management of cultural assets. Increasingly intense rainfall due to climate change will raise the risk of rills/gully erosion [48] and landslides [49, 50]).

The methodology used was primarily focused on assessing the spatial extent and intensity of soil loss and deposition. The USPED empirical model was built by integrating a set of erosion-influencing parameters. USPED's spatial flexibility allows it to model physical erosion processes in a GIS setting. The model can estimate average yearly soil loss and deposition rates, which can then be connected with the archeological sites' topography.

The USPED maps for the different periods considered were intersected with the vulnerability maps given by the KDE (Figs. 2, 3 and 4). As shown in the results, there is different behavior on the areas under erosion/deposition for the different years considering the various degree of vulnerabilities. In conclusion, the paper shows: 1) how the USPED model is greatly affected by differences in the input data (in this case land use) (Fig. 8); 2) how climate change (modelled with rainfall events with the same amount of rainfall but at a shorter time - extreme events) has a fundamental role in the amount of soil erosion/deposition that is very dangerous for the conservation of archaeological sites in the Sinni basin. This is especially visible for the maximum erosion/deposition classes, which have a 20% increase in vulnerable areas compared to 2023 (Table 2 and Fig. 8). This value shows how climate change may endanger many sites/areas/monuments of archaeological interest that do not currently show vulnerability to erosion.

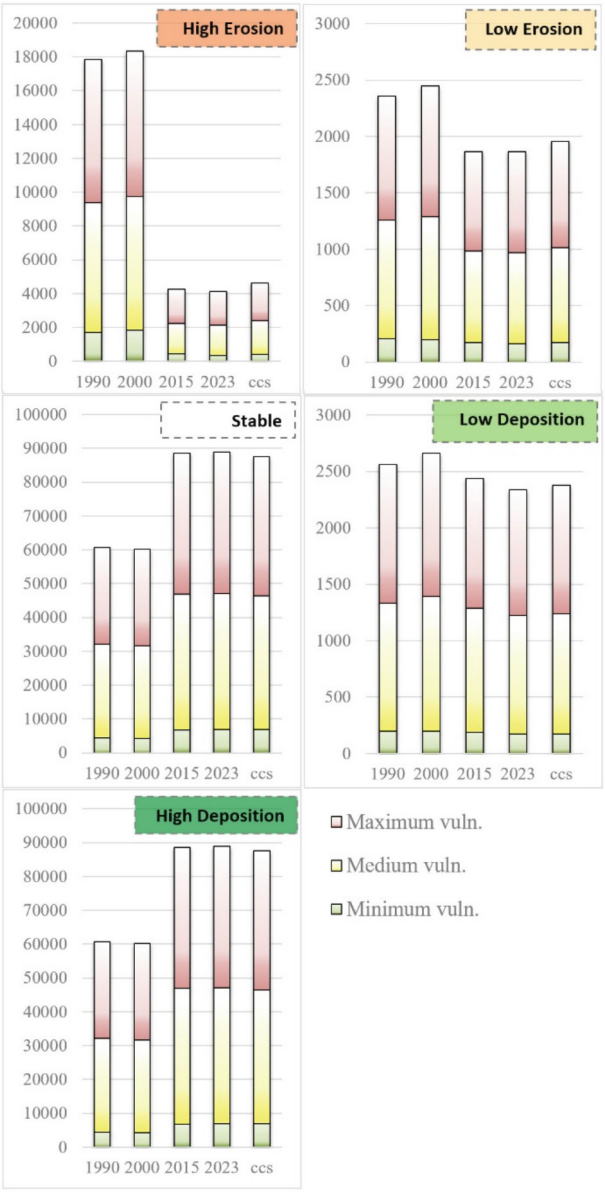

Fig. 8. Comparison between the different classes of USPED model found (in ha), calculated in the different years and scenarios and for the three vulnerability classes.

In this regard, the current study is one of the first to investigate the influence of both erosion-related processes on archeological sites.

Acknowledgments. This study was funded under the project "Study of hazard elements and their variation as a function of climate change, on cultural heritage using spatial machine learning methods" inside "Cultural heritage and creativity in green and digital transitions for inclusive societies" (FOE2021 - Ordinary fund for research organizations and institutions) .

Disclosure of Interests. The authors have no competing interests to declare that are relevant to the content of this article.

References

1. Bilotta, E., Flora, A., Lirer, S., Viggiani, C.: Geotechnics and heritage: Case histories (2013)
2. Gill-Robinson, H.: Managing wetland archaeology: environmental degradation at wetland archaeological sites. Managing Archaeological Resources: Global Context, National Programs, Local Actions, pp. 233–240 (2016)
3. Sala, M., Alcamo, G., Nelli, L.C.: Sustainable strategies for protecting and managing cultural heritages: the case study of Gonfienti in the Tuscany region of Italy. Mediterranean Green Buildings and Renewable Energy: Selected Papers from the World Renewable Energy Network's Med Green Forum, pp. 33–46 (2017)
4. Hemo, E., Linn, R.: Sustainable conservation of archaeological sites with local communities: the case study of tel Yoqne'am, Israel. J. Eastern Mediterranean Archaeol. Heritage Stud. **5**, 411–426 (2017)
5. De Man, A., Tavares, J.T.: Small site conservation in the scope of territorial cohesion. In: AIP Conference Proceedings (2023)
6. Lillak, A.: Nature management and protection of archaeological sites in Estonia. Internet Archaeol. (2023)
7. Fatorić, S., Seekamp, E.: Are cultural heritage and resources threatened by climate change? A systematic literature review. Clim. Change **142**, 227–254 (2017)
8. Sesana, E., Gagnon, A.S., Ciantelli, C., Cassar, J., Hughes, J.J.: Climate change impacts on cultural heritage: a literature review. Wiley Interdisciplinary Reviews: Climate Change 12 (2021)
9. Agapiou, A., Lysandrou, V., Hadjimitsis, D.G.: A European-scale investigation of soil erosion threat to subsurface archaeological remains. Remote Sens. 12 (2020)
10. Howland, M.D., Jones, I.W.N., Najjar, M., Levy, T.E.: Quantifying the effects of erosion on archaeological sites with low-altitude aerial photography, structure from motion, and GIS: a case study from southern Jordan. J. Archaeol. Sci. **90**, 62–70 (2018)
11. Banks, R., Fradley, M., Schiettecatte, J., Zerbini, A.: An integrated approach to surveying the archaeological landscapes of Yemen. Proc. Seminar Arab. Stud. **47**, 9–23 (2017)
12. Kibblewhite, M., Tóth, G., Hermann, T.: Predicting the preservation of cultural artefacts and buried materials in soil. Sci. Total. Environ. **529**, 249–263 (2015)
13. Merritt, W.S., Letcher, R.A., Jakeman, A.J.: A review of erosion and sediment transport models. Environ. Model. Softw., 761–799 (2003)
14. Minervino Amodio, A., Gioia, D., Danese, M., Masini, N., Sabia, C.A.: Land-Use Change Effects on Soil Erosion: The Case of Roman "Via Herculia" (Southern Italy)—Combining Historical Maps, Aerial Images and Soil Erosion Model. Sustainability (Switzerland) 15 (2023)
15. Danese, M., Lazzari, M., Murgante, B.: Kernel density estimation methods for a geostatistical approach in seismic risk analysis: the case study of Potenza Hilltop Town (Southern Italy). In: Lecture Notes in Computer Science (including subseries Lecture Notes in Artificial Intelligence and Lecture Notes in Bioinformatics), pp. 415–429 (2008)

16. Mitasova, H., Hofierka, J., Zlocha, M., Iverson, L.R.: Modelling topographic potential for erosion and deposition using GIS. Int. J. Geogr. Inf. Syst. **10**, 629–641 (1996)
17. Harmon, B.A., Mitasova, H., Petrasova, A., Petras, V.: R.sim.terrain 1.0: A landscape evolution model with dynamic hydrology. Geoscientific Model Dev. **12**, 2837–2854 (2019)
18. Capolongo, D., Diodato, N., Mannaerts, C.M., Piccarreta, M., Strobl, R.O.: Analyzing temporal changes in climate erosivity using a simplified rainfall erosivity model in Basilicata (southern Italy). J. Hydrol. **356**, 119–130 (2008)
19. Gioia, D., Minervino Amodio, A., Maggio, A., Sabia, C.A.: Impact of Land Use Changes on the Erosion Processes of a Degraded Rural Landscape: An Analysis Based on High-Resolution DEMs, Historical Images, and Soil Erosion Models. Land, vol. 10, (2021)
20. Renard, K.G., Foster, G.R., Weesies, G.A., Mccool, D.K., Yoder, D.C.: Predicting soil erosion by water: a guide to conservation planning with the Revised Universal Soil Loss Equation (RUSLE) (1997)
21. Capolongo, D., Pennetta, L., Piccarreta, M., Fallacara, G., Boenzi, F.: Spatial and temporal variations in soil erosion and deposition due to land-levelling in a semi-arid area of Basilicata (Southern Italy). Earth. Surf. Proc. Land. **33**, 364–379 (2008)
22. Robinson, D.A., Phillips, C.P.: Crust development in relation to vegetation and agricultural practice on erosion susceptible, dispersive clay soils from central and southern Italy. Soil and Tillage Research **60**, 1–9 (2001)
23. Wischmeier, W.H., Smith, D.D.: Predicting rainfall erosion losses: a guide to conservation planning (1978)
24. Renard, K.G., Foster, G.R.: Soil conservation: principles of erosion by water (1983)
25. Vezzani, L.: Il bacino plio-pleistocenico di S. Arcangelo (Lucania). In: Atti Ac. Gioenia di Scienze Naturali di Catania, pp. 207–227. Tipog. Zuccarello & Co., (1967)
26. Quilici Gigli, S., WQuilici, L.: Carta Archeologica della valle del Sinni, Roma (2003)
27. Quilici Gigli, S., WQuilici, L.: Carta Archeologica della valle del Sinni. Da Valsinni a San Giorgio Lucano e Cersosimo, Roma (2002)
28. Quilici Gigli, S., WQuilici, L.: Carta Archeologica della valle del Sinni. Dalle colline di Noepoli ai monti Colobraro, Roma (2002)
29. Quilici Gigli, S., WQuilici, L.: Carta Archeologica della valle del Sinni. Zona di Senise, Roma (2001)
30. Quilici Gigli, S., WQuilici, L.: Carta Archeologica della valle del Sinni. Da Castronuovo di S. Andrea a Chiaromonte, Calvera, Teana e Fardella, Roma (2001)
31. Quilici Gigli, S., WQuilici, L.: Carta Archeologica della valle del Sinni. Il massiccio del Pollino e le colline di Francavilla in Sinni, San Costantino Albanese, San Severino Lucano, Agromonte Magnano e Mileo, Roma (2001)
32. Quilici Gigli, S., WQuilici, L.: Carta Archeologica della valle del Sinni. Da Episcopia a Latronico a Seluci e Monte Sirino., Roma (2003)
33. Quilici Gigli, S., WQuilici, L.: Carta Archeologica della valle del Sinni. Documentazione cartografica, Roma (2003)
34. De Angeli, S., Battistin, F.: Archaeological site monitoring and risk assessment using remote sensing technologies and GIS. A Research Agenda for Heritage Planning: Perspectives from Europe, pp. 145–154 (2021)
35. Danese, M., Masini, N., Biscione, M., Lasaponara, R.: Predictive modeling for preventive archaeology: overview and case study. Central Eur. J. Geosci., 42–55 (2014)
36. Di Leo, P., et al.: Ancient settlement dynamics and predictive archaeological models for the Metapontum coastal area in Basilicata, southern Italy: from geomorphological survey to spatial analysis. J. Coast. Conserv. **22**(5), 865–877 (2017). https://doi.org/10.1007/s11852-017-0548-y

37. Schiattarella, M., Giannandrea, P., Corrado, G., Gioia, D.: Landscape planning-addressed regional-scale mapping of geolithological units: an example from Southern Italy. J. Maps **20**, 2303335 (2024)
38. Colette, A.: Climate change and world heritage: report on predicting and managing the impacts of climate change on world heritage and Strategy to assist States Parties to implement appropriate management responses. UNESCO (2007)
39. UNESCO: Policy document on the impacts of climate change on World Heritage Properties. UNESCO (2008)
40. Pickles, D., et al.: Flooding and Historic Building. In: England, H. (ed.), p. 47 (2015)
41. Cassar, M., Sabbioni, C., Brimblecombe, P.: The Atlas of climate change impact on European cultural heritage. In: Commission, E. (ed.). Anthem Press (2010)
42. Blankholm, H.P.: Long-term research and cultural resource management strategies in light of climate change and human impact. Arct. Anthropol. **46**, 17–24 (2009)
43. Kincey, M., Challis, K., Howard, A.J.: Modelling selected implications of potential future climate change on the archaeological resource of river catchments: an application of geographical information systems. Conserv. Manage. Archaeol. Sites **10**, 113–131 (2008)
44. Ravankhah, M., et al.: Integrated assessment of natural hazards, including climate change's influences, for cultural heritage sites: the case of the historic centre of rethymno in Greece. Int. J. Disaster Risk Sci. **10**, 343–361 (2019)
45. Wang, J.-J.: Flood risk maps to cultural heritage: measures and process. J. Cult. Herit. **16**, 210–220 (2015)
46. Mattei, G., Rizzo, A., Anfuso, G., Aucelli, P.P.C., Gracia, F.J.: A tool for evaluating the archaeological heritage vulnerability to coastal processes: the case study of Naples Gulf (southern Italy). Ocean Coast. Manage. **179**, 104876 (2019)
47. Di Paola, G., Minervino Amodio, A., Dilauro, G., Rodriguez, G., Rosskopf, C.M.: Shoreline evolution and erosion vulnerability assessment along the central Adriatic coast with the contribution of UAV beach monitoring. Geosciences **12** (2022)
48. Nicu, I.C.: Cultural heritage assessment and vulnerability using analytic hierarchy process and geographic information systems (Valea Oii catchment, North-eastern Romania). An approach to historical maps. Int. J. Disaster Risk Reduction **20**, 103–111 (2016)
49. Gariano, S.L., Guzzetti, F.: Landslides in a changing climate. Earth Sci. Rev. **162**, 227–252 (2016)
50. Gioia, D., Corrado, G., Minervino Amodio, A., Schiattarella, M.: Multi-temporal morphological analysis coupled to seismic survey of a mass movement from southern Italy: a combined tool to unravel the history of complex slow-moving landslides. Natural Hazards, PREPRINT (2023)